# COMPARISON OF THE USE OF SENTINEL-1 SAR AND ALOS-2 PALSAR-2 IN MANGROVE ABOVEGROUND BIOMASS ESTIMATION IN SAN JUAN, BATANGAS, PHILIPPINES

J. J. Bilolo [1] *, J. V. Dida [1], and A. Araza [2]

[1] Institute of Renewable Natural Resources, College of Forestry and Natural Resources, University of the Philippines Los Baños, College, Laguna 4031 Philippines – (jjbilolo, jvdida) @up.edu.ph
[2] Environmental Systems Analysis, Environmental Sciences Group, Wageningen University and Research, Droevendaalsesteeg 3, 6708 PB Wageningen, The Netherlands - arnan.araza@wur.nl

**KEY WORDS:** Mangroves, Aboveground Biomass Estimation, Remote Sensing, Sentinel-1, ALOS-2 PALSAR-2

**ABSTRACT:**

This study compares the potential of Sentinel-1 and ALOS-2 PALSAR-2 in estimating mangrove aboveground biomass (AGB) in San Juan, Batangas, Philippines. Mangrove forests are essential coastal ecosystems that are facing growing threats. One way of conserving them is by creating policies that can protect them. To do this effectively, information like AGB can be used as a guide. However, conventional AGB estimations are labor-intensive and ecologically disruptive. Conversely, remote sensing technologies, such as synthetic aperture radar (SAR), offer a more efficient alternative. Sentinel-1, operating in C-band, and ALOS-2 PALSAR-2, operating in L-band, are two prominent SAR platforms with global coverage, offering data for land cover classification, forest monitoring, and forest biomass estimation. This research used the backscatter values of Sentinel-1 and ALOS-2 PALSAR-2 as predictor variables in estimating mangrove AGB by correlating them to the observed AGB from a mangrove survey. The models developed using these platforms yielded limited accuracy, with low coefficient of determination ($R^2$) (Sentinel-1 = 0.13; ALOS-2 PALSAR-2 = 0.12) and RMSE (Sentinel-1 = 8.72 Mg $ha^{-1}$; ALOS-2 PALSAR-2 = 8.78 Mg $ha^{-1}$). Potential sources of errors were identified, including small sample size and data noise. On the results, Sentinel-1 demonstrates a slightly better performance in terms of the $R^2$ and RMSE in the modeling while ALOS-2 PALSAR-2 performed better in the validation, however, both still yielded suboptimal AGB estimates compared to other studies. Refining the models by incorporating additional parameters, exploring machine learning, and considering other data sources are recommended to enhance AGB estimation.

## 1. BACKGROUND

Located in the easternmost part of the province of Batangas, Philippines, the Municipality of San Juan is home to one of the largest mangrove forests in its province. However, recent reports from the municipal government in 2022 indicate that the mangroves of San Juan are confronting several challenges stemming from illegal and unregulated utilization of mangrove resources, as well as ineffective local management practices.

Mangrove forests are vital intertidal ecosystems that exist in coastal environments across tropical, subtropical, and temperate regions. They serve multiple crucial functions, including the preservation of coastal biodiversity, the mitigation of climate change impacts, and the support of local livelihoods (Donato *et al.*, 2011). Moreover, mangroves have been found to sequester and deposit carbon in their biomass and soils at a significantly higher rate than terrestrial forests, with estimates ranging between two and five times more (Alongi, 2012). Despite their immense ecological value though, these essential ecosystems face escalating threats due to human activities (Friess *et al.*, 2019).

Biomass pertains to a living thing's mass, which includes flora, fauna, and microorganisms (Houghton, 2008). In a mangrove forest, biomass is generally found in several pools, mainly aboveground, belowground, necromass, and soil biomass. Aboveground biomass, especially, is considered important as it serves as an indicator of the aboveground structure of the forest and its productivity (Zhang *et al.*, 2016 as cited in Nizamani *et al.*, 2021).

Conventional methods used to study mangroves, especially mangrove biomass, such as field surveys and non-destructive sampling, as employed by Gevana *et al.* (2008) and Gevana and Pampolina (2009) in their research on the area, are labor-intensive and have ecological impacts. In contrast, remote sensing technologies, specifically, synthetic aperture radar (SAR) imaging, offer a promising, non-invasive, and more efficient approach to estimating mangrove biomass, presenting an alternative to the labor-intensive and costly traditional methods.

SAR imaging, like other remote sensing platforms allows for assessments over large spatial scales, enabling researchers to obtain valuable information without extensive on-the-ground work (Kumar *et al.*, 2015). It relies on signal-processing techniques to create an extended effective antenna rather than employing a physically large antenna (Cutrona, 1990).

By leveraging synthetic aperture radar data, researchers can analyze the backscattering properties of mangrove forests, which provide insights into their structure, density, and biomass. This non-invasive approach allows for the estimation of aboveground biomass without directly disturbing the mangroves themselves (Ghasemi *et al.*, 2011).

ALOS-2 PALSAR-2 and Sentinel-1 are two prominent SAR platforms used for remote sensing applications. ALOS-2 PALSAR-2, or the Phased Array type L-band Synthetic Aperture Radar 2 aboard the Advanced Land Observing Satellite 2, launched by the Japan Aerospace Exploration Agency (JAXA) in 2014, operates in L-band frequency (1.2 GHz) and offers high-

* Corresponding author

resolution SAR imagery with single (HH or VV) or double polarization (HH/HV or VV/VH). It provides valuable data for land cover classification, forest monitoring, disaster management, forest biomass, and deforestation (EORC & JAXA, 2007).

On the other hand, Sentinel-1, developed by the European Space Agency (ESA) and launched in 2014, consists of a constellation of SAR satellites. It operates in C-band (5.405 GHz) and offers dual-polarization (HH+HV, VV+VH) capabilities, allowing for enhanced data analysis. Sentinel-1 data is widely used for applications such as maritime surveillance, agriculture monitoring, and ice mapping (Bourbigot *et al.*, 2016).

Both platforms provide frequent global coverage, making them valuable resources for monitoring and research. Their SAR imaging capabilities enable the acquisition of data in all weather conditions, day, or night, allowing for consistent and reliable observations.

With that, this research aims to explore the potential of Sentinel-1 and ALOS-2 PALSAR-2 in capturing the biomass variations within mangrove forests by comparing their performance. The difference in the wavelengths of these two allows for differing penetration depths and sensitivities to the structural and compositional variations of the mangrove canopies (Saatchi, 2019). By evaluating the relationship between radar signals and actual biomass measurements on the ground, this study seeks to refine and validate the capabilities of remote sensing technology for mangrove monitoring. Furthermore, the information that will be derived from this study can be used in enhancing policies for managing and protecting threatened resources such as mangrove forests.

## 2. MATERIALS AND METHODOLOGY

### 2.1 Study Area

San Juan is a coastal town on the eastern tip of Batangas, Philippines (Figure 1). It currently has 185.75 ha of mangrove forests, separated into two major locations in the northeastern and southeastern parts of the municipality. For this study, the mangroves in the southeastern part which are primarily coastal, were selected.

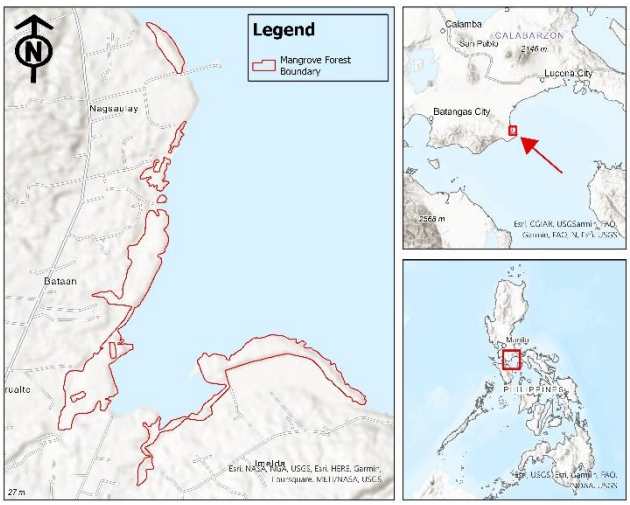


**Figure 1.** Location of the study site. Basemap: © Esri World Terrain with Labels

The 84.28-hectare southern mangrove stand was delineated using the 2015 National Land Cover Map from the National Mapping and Resource Information Agency (NAMRIA) (2015). The stand is primarily located on the coast of Coloconto Bay, which is part of the larger Tayabas Bay and is shared by five barangays, including Subukin, Nagsaulay, Bataan, Barualte, and Imelda.

### 2.2 SAR imagery

Two types of SAR images were used in this study.

**2.2.1 Sentinel-1 data and processing**: The first one is Sentinel-1 which is primarily operated by the European Space Agency (ESA). A total of 16 images collected from August 2, 2022, to January 29, 2023, were freely downloaded from the Copernicus Sentinel Open Access Hub.

These images were first preprocessed using the ESA-SNAP Desktop application, v. 3.2.1, and following the Sentinel-1 Toolbox Tutorials by Braun & Veci (2015/2021) on SAR Basics and Time-series Analysis as well as the SAR Pre-processing Documentation of Weiß (2019). The preprocessing was composed of the extraction of the initial subset of the Sentinel-1 images to reduce the load that the computer and the processing software will work on. It was followed by the application of an Orbit File, with Sentinel Precise (Auto-Download) orbit state vector and polynomial state of 3. The next step was the Radiometric Calibration where a Sigma0 output was derived. It was followed by the Range-Doppler Terrain Correction which used the SRTM 1Sec HGT (Auto Download) for the digital elevation model (DEM), bilinear interpolation for the DEM and image resampling method, and UTM Zn 51N for the map projection. Furthermore, the option to mask out areas without elevation was also unchecked. After those processes, another subset was extracted. This will be the final subset that will be used in the post-processing. This was done as the images still shifted during the preprocessing which caused the initial subset to misalign slightly.

For the postprocessing, the 16 Sentinel-1 images were Stacked, and the Refined Lee multi-temporal filter was applied. The Refined Lee filter is the refined version of the Lee Filter which reduces the speckle of a radar image by preserving the image sharpness and detail (Quegan *et al.*, 2000; Yommy *et al.*, 2015). Compared to the latter, the former uses a damping factor and the number of looks in its algorithm. This was used as it limits the speckle in the image while still preserving the texture information (Esri, 2021). Subsequently, Data Stack Averaging was conducted. This computes the mean of pixels of multitemporal images. This results in a single image where each pixel's value is the average of all the pixels of all other pixels in its stack. Lastly, the resulting values in linear scale were converted to decibels before extracting them.

**2.2.2 ALOS-2 PALSAR-2 data and processing**: On the other hand, for the second type of data, the open-access Global PALSAR-2/PALSAR Yearly Mosaic, version 2 from the Japan Aerospace Exploration Agency (JAXA) (dated January 1, 2017, to January 1, 2018) in the Google Earth Engine Catalog was used. It was first preprocessed in ArcGIS Pro v. 3.2.0 by resampling the downloaded image with 25 m resolution to 10 m to ensure that it has the same size as the sampling plots used in the study. The Bilinear Method was used in the process as this method is best for continuous data with no distinct boundaries as it gradually smooths out data of this type but not as much as with cubic convolution (GISGeography, 2023). Furthermore, an

initial subset of the image was also extracted to lighten the processing burden of the computer used. Subsequently, the backscatter values of ALOS-2 PALSAR-2 in 16-bit digital numbers (DN) were converted to $\sigma^0$ using the formula (Rosenqvist, 2007):

$$\sigma^0 = 10*\log_{10}(DN^2) - 83.0 \text{ dB} \quad (1)$$

where $\sigma^0$ = converted to sigma naught values in decibels (dB)
DN = 16-bit digital numbers (DN)

Forty-two pixels, with 10 m resolution, within the study area were randomly selected to be used as the sampling plots. Of those, 32 were used as modeling plots while the remaining 10 were for validation.

### 2.3 Observed Mangrove AGB

For the observed mangrove AGB, a total of 42 10 m × 10 m sampling plots with the same geographic coordinates as with the pixels in the SAR images were used. Similarly, thirty-two of the sampling plots will be used as modeling plots while the remaining 10 will be for validation. The genus name and diameter at the breast height (dbh) of all the mangroves inside the chosen plots were collected. Furthermore, the wood density of the identified mangrove genus was determined by averaging wood density values from various species within the same genus obtained from published studies and manuals.

The gathered data were used in the computation of the observed AGB of the sampling plots. The general formula for mangrove AGB developed by Komiyama *et al.* (2005) was used (Formula 2).

$$B = 0.251\rho(DBH)^{2.46} \quad (2)$$

where $\rho$ = wood density (g $cm^{-3}$)
DBH = diameter at breast height (cm)

The equation was used since the site has a similarly diverse set of mangrove species as the one used by Komiyama *et al.* (2005). Furthermore, the equation also fits the range of mangrove DBH measured from the study site (5 cm to 49 cm). Lastly, with an $R^2$ of 0.98, this formula may be reliable in estimating the AGB at the study site.

### 2.4 Model fitting and validation of predictions

Regression models that correlated backscatter values and AGB of the 32 field plots (observed AGB) were conducted. For the Sentinel-1 image, the ratio (VV/VH)/(VH/VV) of the backscatter values from the available polarizations was used and correlated with the observed AGB values. This backscatter ratio was selected from several ratios of VV to VH values that were tested. On the other hand, the converted backscatter values from the HH polarization of ALOS-2 PALSAR-2 were used and correlated with observed AGB values from the study site. The coefficient of determination ($R^2$) and the root mean square error (RMSE) were used in the comparison of the accuracy of the mangrove AGB predictions produced from the two. $R^2$ and RMSE were computed using the following formulae, respectively:

$$R^2 = 1 - (RSS/TSS) \quad (3)$$

where $R^2$ = coefficient of determination
RSS = sum of squares of residuals
TSS = total sum of squares

$$RMSE = SQRT[\Sigma i(y_i-y_{i'})^2/n] \quad (4)$$

where $y_i$ = observed AGB
$y_{i'}$ = predicted AGB from Sentinel-1 and PALSAR-2 backscatter values
n = number of plots

Subsequently, the validation of the AGB predictions from the regression model was done. The formula of the best-fitting trendline, polynomial, was used to predict the AGB using the SAR backscatter values. Another regression analysis was done comparing the predicted AGB from SAR backscatter values and the observed AGB from the 10 remaining validation plots. The $R^2$ and RMSE of each model were used again to compare the accuracy of the two platforms.

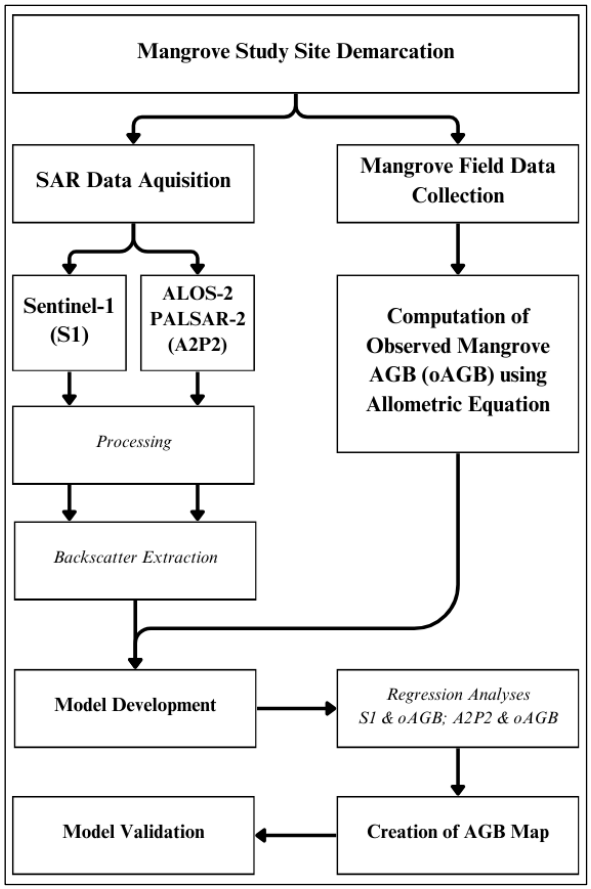


**Figure 2**. Flowchart of the major steps in the AGB estimation, map generation, and model validation done in this study.

## 3. RESULTS AND DISCUSSION

### 3.1 Observed Mangrove AGB

A total of 1,308 mangroves were recorded from the forty-two 10 m × 10 m sampling plots that were randomly selected at the study site. This was divided into two groups: 32 plots were used for the modeling with 737 mangroves while the remaining 10 plots with 301 mangroves were used for the validation of the model. The range of mangroves measured in each plot is from 4 to 62 trees.

Furthermore, seven genera of mangrove species were identified in the survey while 15 mangroves that were not identified were

included in a "Miscellaneous" classification. Table 1 shows the summary of the average wood density of each mangrove genus that was identified in the study. In the case of the "Miscellaneous" classification, the wood density of the other 8 genera was averaged instead.

| Mangrove Genera | Average Wood Density (g $cm^{-3}$) |
|---|---|
| *Aegiceras* | 0.6784 |
| *Avicennia* | 0.5868 |
| *Bruguierra* | 0.7802 |
| *Ceriops* | 0.7355 |
| *Rhizophora* | 0.7703 |
| *Sonneratia* | 0.4100 |
| *Xylocarpus* | 0.5295 |
| Miscellaneous | 0.6415 |

**Table 1**. Summary of the mangrove wood density used in the computation of observed AGB (Komiyama *et al*., 1988; Komiyama *et al*., 2000, as mentioned in Komiyama *et al*., 2005; Simpson, 1996; Tamai *et al*., 1986; and World Agroforestry Centre as mentioned in Kauffman and Donato, 2012).

The average DBH for each plot ranged from 6.6 cm to 25.8 cm while the wood densities used had a minimum of 0.41 g $cm^{-3}$ and a maximum of 0.7802 g $cm^{-3}$ with an average of 0.6415 g $cm^{-3}$. Lastly, the total observed AGB in Mg $ha^{-1}$ ranged from 1.705 Mg $ha^{-1}$ to 45.327 Mg $ha^{-1}$ with an average of 17.241 Mg $ha^{-1}$ (Figure 3).

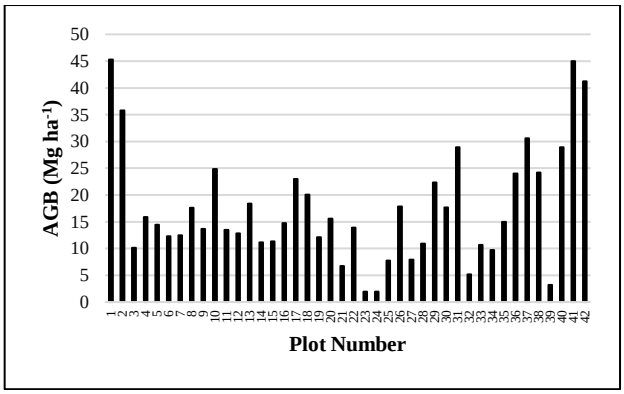


**Figure 3**. Observed mangrove aboveground biomass for each plot that was computed using the general formula of Komiyama *et al.* (2005).

### 3.2 Backscatter Values

**3.2.1 Sentinel-1 backscatter values**: The Sentinel-1's backscatter values for each plot used in modeling are shown in Figure 4. For VV backscatter values, the average is -8.64 dB, with a minimum of -10.66 dB and a maximum of -6.54 dB, while for the VH backscatter values, the average is -13.995 dB, with a maximum of -16.35 dB and a maximum of -12.09 dB.

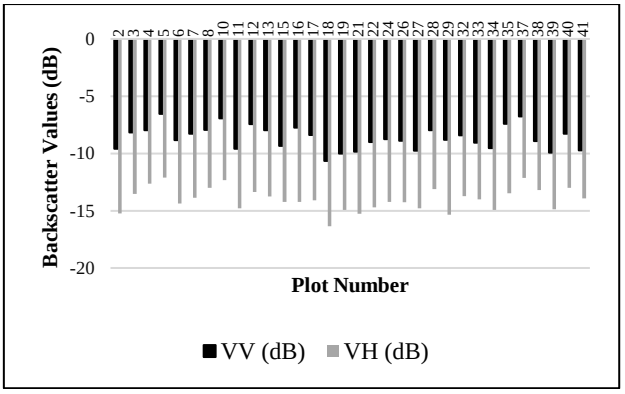


**Figure 4**. Sentinel-1 backscatter values of the modeling plots.

**3.2.2 ALOS-2 PALSAR-2 backscatter values**: For ALOS-2 PALSAR-2, the backscatter values from HH polarization were used in this study (Figure 5). The average backscatter value for this dataset is -9.19 dB with a minimum value of -13.57 dB and a maximum value of -4.89 dB.


**Figure 5**. ALOS-2 PALSAR-2 HH polarization backscatter values of the modeling plots.

### 3.3 Regression Results

The regression analyses between the predictor variables and the observed AGB from the surveyed mangroves are shown in Figures 6 and 7. For Sentinel-1, the backscatter ratio (VV/VH)/(VH/VV) was used as the predictor variable and was regressed with the observed AGB.

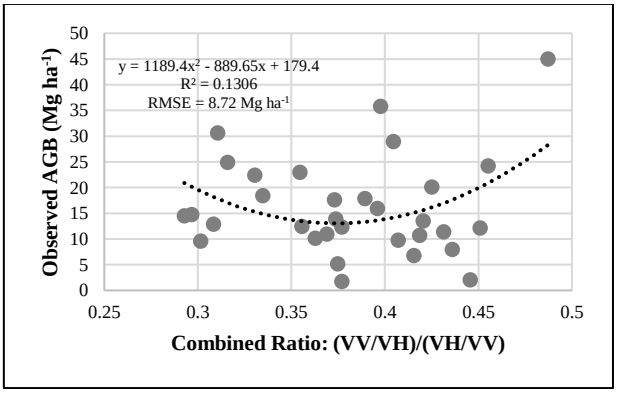


**Figure 6**. Regression Result between observed mangrove AGB and the combined ratio of Sentinel-1 VV and VH polarization backscatter values.

On the other hand, the HH backscatter values were used as the predictor variable for the ALOS-2 PALSAR-2 and were regressed, also with the observed mangrove AGB.

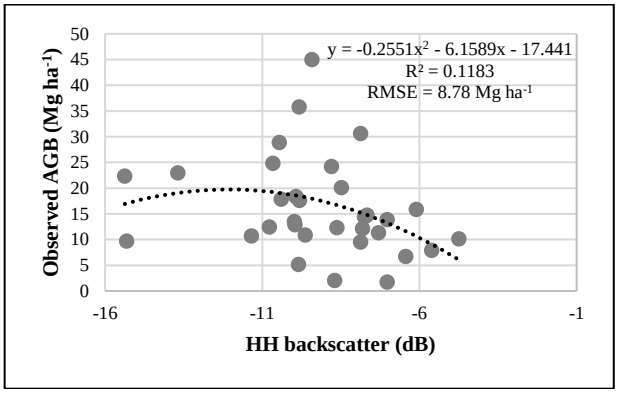


**Figure 7**. Regression Result between observed mangrove AGB and the ALOS-2 PALSAR-2 HH polarization backscatter values.

Figure 6 and 7 shows the results between Sentinel-1 and ALOS-2 PALSAR-2 regression with the observed mangrove AGB. On the other hand, Table 2 summarizes the results of the regression between the observed AGB and the predictor variables. Looking at the results, Sentinel-1 yields a slightly higher $R^2$ than that of ALOS-2 PALSAR-2. The former, using the backscatter ratio, resulted in an $R^2$ of 0.13 while the latter using only HH backscatter values resulted in 0.12, both were achieved using polynomial regression. Furthermore, Sentinel-1 resulted also in a slightly better RMSE of 8.72 Mg ha$^{-1}$ while for ALOS-2 PALSAR-2, the RMSE was 8.78 Mg ha$^{-1}$.

| Predictor Variables | Equation | $R^2$ | RMSE (Mg ha$^{-1}$) |
|---|---|---|---|
| (VV/VH)/ (VH/VV) | $y = 1189.4x^2 - 889.65x + 179.4$ | 0.13 | 8.72 |
| HH | $y = -0.2551x^2 - 6.1589x - 17.441$ | 0.12 | 8.78 |

**Table 2**. Summary of the result of the polynomial regression between the observed mangrove AGB and predictor variables.

### 3.4 Aboveground Biomass Map

Using the models derived from the regression analysis conducted between the predicted variables and the backscatter values from Sentinel-1 and ALOS-2 PALSAR-2, aboveground biomass maps of the study were generated (Figures 8 and 9).

For the Sentinel-1 generated map (Figure 8), the AGB values in the study area range between 184.74 Mg ha$^{-1}$ and 314.53 Mg ha$^{-1}$ while the average AGB is 249.64 Mg ha$^{-1}$. Notably, some areas yielded predictions with extreme values, especially those at the edges of the forest. According to Simard (2019), this can be attributed to double-bounce scattering—which occurs when radio waves bounce off surfaces and direct them back to the sensor, such as vertical stems and aerial roots—which is exacerbated by the inundation of the area. Furthermore, this phenomenon can also be observed in areas with open canopies as these areas expose the stems and aerial roots of mangroves as well which can allow for double-bounce scattering.

On the other hand, for the ALOS-2 PALSAR-2 AGB map (Figure 9), the predictions range from values between 0 and 19.73 Mg ha$^{-1}$ with an average AGB of 9.87 Mg ha$^{-1}$. Unlike the results from the Sentinel-1 AGB map, no case of extremely high values due to double-bounce scattering and inundation was observed. Additionally, the generated map also corresponds to the site conditions of the area as it also mirrors the density of vegetation observed during the mangrove survey, something that can't be said with the generated map from Sentinel-1 map.

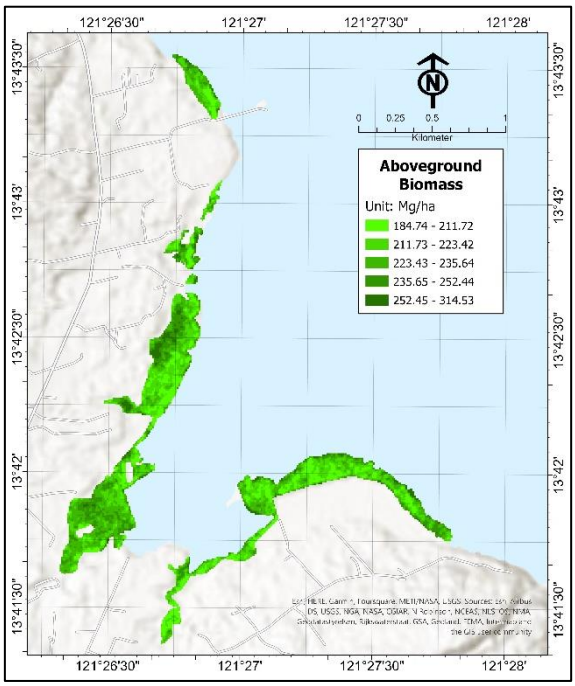


**Figure 8**. Mangrove AGB map of the study site using Sentinel-1. Basemap: © Esri World Terrain with Labels

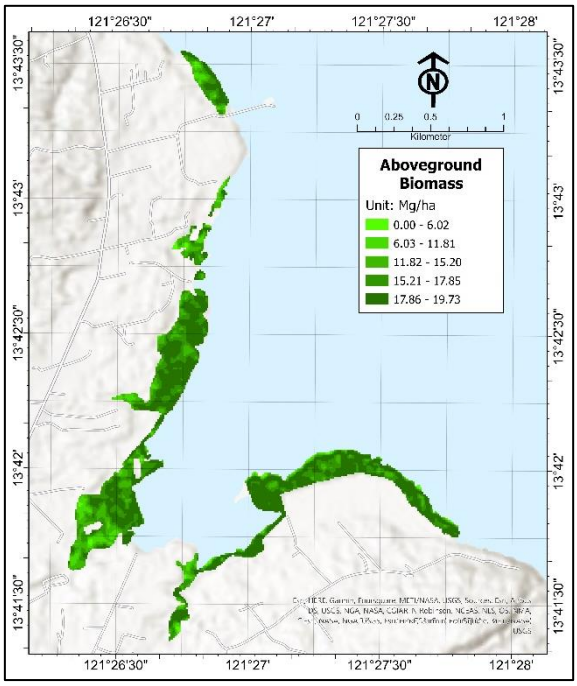


**Figure 9**. Mangrove AGB map of the study site using ALOS-2 PALSAR-2. Basemap: © Esri World Terrain with Labels

### 3.5 Model Validation

To assess the accuracy of the AGB maps, ten separate 10 m × 10 m validation plots, distinct from the 32 modeling plots, were used. These validation plots allowed for the correlation of the

estimated AGB from the developed models with samples collected outside the modeling plots.

Figure 10 shows the clustered column charts of all the validation plots and the predicted AGB from Sentinel-1 and ALOS-2 PALSAR-2 in comparison to the observed AGB. As seen, Sentinel-1 predictions are a lot greater than that of ALOS-2 PALSAR-2, and in general, the latter has closer values to the observed AGB than the former.

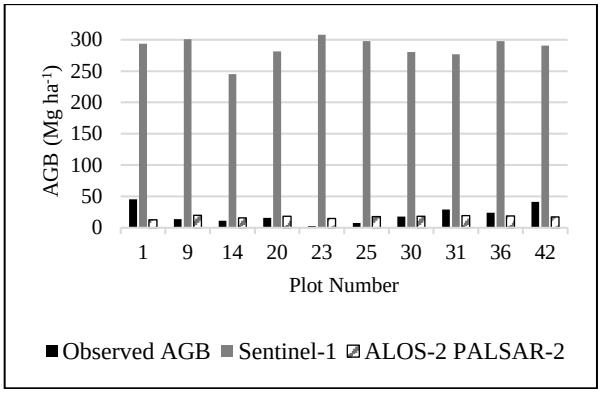


**Figure 10**. Comparison between observed AGB and predicted AGB from the generated map

On the other hand, Figures 11 and 12 depict scatter plots used in the validation of the models, comparing observed AGB with predicted AGB generated using Sentinel-1 and ALOS-2 PALSAR-2 data.

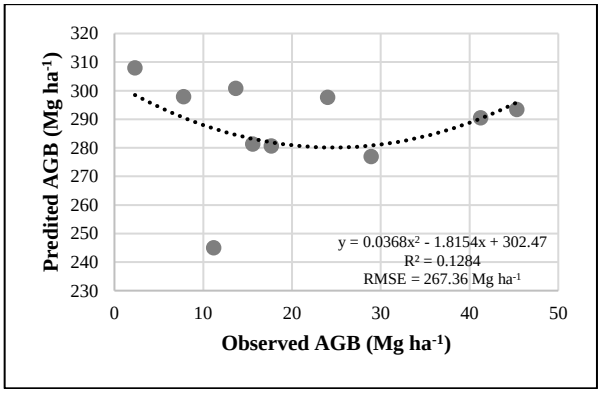


**Figure 11**. Scatter plot between the observed AGB and predicted AGB in the map generated from Sentinel-1 data.

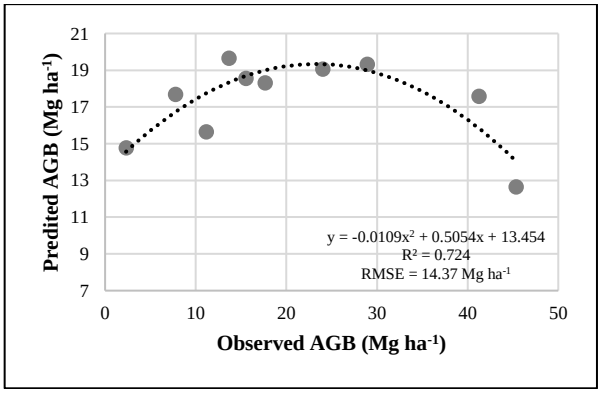


**Figure 12**. Scatter plot between the observed AGB and predicted AGB in the map generated from ALOS-2 PALSAR-2 data.

Sentinel-1 achieved an $R^2$ of 0.13 with an RMSE of 267.36 Mg $ha^{-1}$, whereas ALOS-2 PALSAR-2 exhibited an $R^2$ of 0.72 with an RMSE of 14.37 Mg $ha^{-1}$. This suggests that despite the Sentinel-1 model having slightly better $R^2$ and RMSE, the model developed for ALOS-2 PALSAR-2 still outperforms it, as it also yielded significantly better results in validation.

However, even with that, the models generated using both platforms still exhibited suboptimal performance. The low coefficient of determination implies that the models are not doing a good job of predicting the expected values in the study, leading to considerable degrees of error present in the model's predictions, and thus, the predicted values are far from the actual values, resulting to inaccurate predictions of the model. On the other hand, it can also be that other factors such as data outliers, data noise, and overlooked errors in the methods used could be the reason why the models do not perform as expected.

With that, in general, ALOS-2 PALSAR-2 still offers a greater potential for improved and effective mangrove AGB estimation compared to Sentinel-1 as supported by previous studies (Huang *et al.*, 2018; Luong *et al.*, 2019; Saatchi, 2019). This advantage stems from its utilization of L-band frequency, which boasts a longer wavelength capable of penetrating deeper into the vertical forest profile. However, studies such as that of Hamdan *et al.* (2014) and Nesha *et al.* (2020) claimed that it alone, and without other parameters to support the modeling, cannot ensure a successful estimation due to limited information that ALOS-2 PALSAR-2 backscatter coefficients can provide despite its superior frequency.

In contrast, Sentinel-1, with its C-band SAR, can only penetrate the upper part of the canopy, and rarely the understory. This distinction results in more representative and accurate data for mangrove AGB estimation using ALOS-2 PALSAR-2.

However, ALOS-2 PALSAR-2, being a commercial platform, can pose budget constraints due to the cost of accessing updated data. On that note, some archived data, like the mosaic used in this study from Google Earth Engine, is available for free, along with other global mosaics on JAXA's ALOS Research and Application Project webpage. In contrast, Sentinel-1, as an open-access platform, offers advantages such as higher temporal and spatial resolution and comes with free processing software. This makes it a more cost-effective choice for agencies and institutions with limited research budgets.

## 4. CONCLUSIONS AND RECOMMENDATIONS

This study compared the potential of Sentinel-1 and ALOS-2 PALSAR-2 in the estimation of mangrove AGB in San Juan, Batangas, Philippines. For Sentinel-1, a ratio of the backscatter values of VV and VH polarization was utilized while for the ALOS-2 PALSAR-2, a resampled raster with HH polarization was used. These backscatter values were correlated with observed mangrove AGB that were collected from 32 sampling plots with 10 m × 10 m area to develop the models, while $R^2$ and RMSE were used to assess the accuracy of the models developed.

With that, the Sentinel-1 model exhibited an $R^2$ of 0.13 and an RMSE of 8.72 Mg $ha^{-1}$ while the ALOS-2 PALSAR-2 model yielded an $R^2$ of 0.12 and an RMSE of 8.78 Mg $ha^{-1}$. In terms of the validation wherein the remaining ten 10 m × 10 m plots were used, Sentinel-1 resulted in an $R^2$ of 0.13 and an RMSE of 267.36

Mg $ha^{-1}$, while ALOS-2 PALSAR-2 yielded an $R^2$ of 0.73 and an RMSE of 14.37 Mg $ha^{-1}$.

Generally, these results are significantly poorer than those from previous studies on the same research area which implies that the models' predictions may have high degrees of uncertainty or variability, reducing their practical usefulness for decision-making or AGB prediction. Furthermore, the models also have a high average prediction error, indicating poor accuracy in estimating the dependent variable. However, the small quantity of data and the potential noise may have also contributed to this suboptimal performance. Overall, this can impact the reliability of the model's predictions and limit its practical applicability.

In consideration of that, these results highlight the need for model refinement. To enhance observed AGB estimation, more sampling plots could be added for a greater number of observed AGB values to be used in training the models. Additionally, parameters like tree height and canopy diameter could be incorporated, along with species- or genus-specific mangrove allometric equations.

For SAR data, exploring alternative methods and algorithms in modeling, like incorporating machine learning in the process could also be done. In addition, consideration of additional data sources, such as those that use high spatial resolution optical remote sensing technologies holds promise. Experimentation with different ratios and combinations of Sentinel-1 backscatter values and exploring various polarizations and polarization ratios for ALOS-2 PALSAR-2 could also be tried to enhance model performance. Also, including cross-polarized data could be explored as it is known for its suitability in forest biomass estimation.

Lastly, checking the degree of alignment of the sampling plots on the ground with the pixels of the SAR images is also recommended to ensure that the ground values correspond to the backscatter values in the pixel of the image used in the regression.

## ACKNOWLEDGEMENTS

The authors would like to extend their gratitude to the Department of Science and Technology-Science Education Institute for supporting the study through the thesis allowance granted through the RA 7867 Science and Technology Undergraduate Scholarships. The authors' gratitude also extends to ESA's Sentinels Scientific Data Hub for the Sentinel-1 SAR data and Google's Earth Engine for the ALOS-2 PALSAR-2 Global Yearly Mosaic data.

## REFERENCES

Alongi, D.M., 2012. Carbon sequestration in mangrove forests. Carbon Manag. 3, 313–322. https://doi.org/10.4155/cmt.12.20

Bourbigot, M., Johnsen, H., and Piantanida, R., 2016. Sentinel-1 Product Definition. European Space Agency.

Braun, A. and Veci, L., 2021. Sentinel-1 Toolbox, 4th ed. Array Systems Computing Inc.

Cutrona, L.J., 1990. Synthetic Aperture Radar, 2nd ed, Radar Handbook.

Donato, D.C., Kauffman, J.B., Murdiyarso, D., Kurnianto, S., Stidham, M., and Kanninen, M., 2011. Mangroves among the most carbon-rich forests in the tropics. Nat. Geosci. 4, 293–297. https://doi.org/10.1038/ngeo1123

Earth Observation Research Center and Japan Aerospace Exploration Agency, 2007. ALOS User Handbook. Japan Aerospace Exploration Agency.

Esri, 2021. Speckle Function.

European Space Agency., 2023. Sentinel-1 SAR Images.

Friess, D.A., Rogers, K., Lovelock, C.E., Krauss, K.W., Hamilton, S.E., Lee, S.Y., Lucas, R., Primavera, J., Rajkaran, A., and Shi, S., 2019. The State of the World's Mangrove Forests: Past, Present, and Future. Annu. Rev. Environ. Resour. 44, 89–115. https://doi.org/10.1146/annurev-environ-101718-033302

Gevana, D., Pulhin, F., and Pampolina, N., 2008. Carbo Stock Assessment of a Mangrove Ecosystem in San Juan, Batangas. J. Environ. Sci. Manag. 11, 15–25.

Gevana, D. and Pampolina, N., 2009. Plant diversity and carbon storage of a Rhizopora stand in Verde Passage, San Juan, Batangas, Philippines. J. Environ. Sci. Manag. 12, 1–10.

Ghasemi, N., Sahebi, M., and Mohammadzadeh, A., 2011. A review on biomass estimation methods using synthetic aperture radar data. Int. J. Geomatics Geosci. 1, 776–788.

GISGeography, 2023. Raster resampling for discrete and continuous data. GIS Geogr.

Hamdan, O., Aziz, H.K., Hasmadi, I.M., 2014. L-band ALOS PALSAR for biomass estimation of Matang Mangroves, Malaysia. Remote Sens. Environ. 155, 69–78. https://doi.org/10.1016/j.rse.2014.04.029

Houghton, R.A., 2008. Biomass. Encycl. Ecol. 448–453. https://doi.org/10.1016/b978-008045405-4.00462-6

Huang, X., Ziniti, B., Torbick, N., and Ducey, M.J., 2018. Assessment of Forest above Ground Biomass Estimation Using Multi-Temporal C-band Sentinel-1 and Polarimetric L-band PALSAR-2 Data. Remote Sens. 10, 1424. https://doi.org/10.3390/rs10091424

Japan Aerospace Exploration Agency and Earth Observation Research Center., 2022. Global PALSAR-2/PALSAR Yearly Mosaic.

Kauffman, J.B. and Donato, D., 2012. Protocols for the measurement, monitoring and reporting of structure, biomass and carbon stocks in mangrove forests. CIFOR. https://doi.org/10.17528/cifor/003749

Komiyama, A., Poungparn, S., and Kato, S., 2005. Common allometric equations for estimating the tree weight of mangroves. J. Trop. Ecol. 21, 471–477. https://doi.org/10.1017/s0266467405002476

Kumar, L., Sinha, P., Taylor, S., and Alqurashi, A.F., 2015. Review of the use of remote sensing for biomass estimation to support renewable energy generation. J. Appl. Remote Sens. 9, 97696. https://doi.org/10.1117/1.jrs.9.097696

Luong, V.N., Tu, T.T., Khoi, A.L., Hong, X., Hoan, T.N., and Thuy, T.L.H., 2019. Biomass Estimation and Mapping of Can Gio Mangrove Biosphere Reserve in South of Viet Nam using ALOS-2 PALSAR-2 Data. Appl. Ecol. Environ. Res. 17, 15–31. https://doi.org/10.15666/aeer/1701\{_}015031

National Mapping and Resource Information Authority, 2015. 2015 Forest Land Cover of the Philippines.

Nesha, M.K., Hussin, Y.A., Van Leeuwen, L.M., Sulistioadi, Y.B., 2020. Modeling and mapping aboveground biomass of the restored mangroves using ALOS-2 PALSAR-2 in East Kalimantan, Indonesia. Int. J. Appl. earth Obs. Geoinf. 91, 102158. https://doi.org/10.1016/j.jag.2020.102158

Nizamani, M.M., Harris, A.J., Cheng, X.L., Zhu, Z.X., Jim, C.Y., and Wang, H.F., 2021. Positive relationships among aboveground biomass, tree species diversity, and urban greening management in tropical coastal city of Haikou. Ecol. Evol. 11, 12204–12219. https://doi.org/10.1002/ece3.7985

Quegan, S., Toan, T. Le, Yu, J., Ribbes, F., and Floury, N., 2000. Multitemporal ERS SAR analysis applied to forest mapping. IEEE Trans. Geosci. Remote Sens. 38, 741–753. https://doi.org/10.1109/36.842003

Rosenqvist, A., Shimada, M., Ito, N., and Watanabe, M., 2007. ALOS PALSAR: a Pathfinder mission for Global-Scale Monitoring of the environment. IEEE Trans. Geosci. Remote Sens. 45, 3307–3316. https://doi.org/10.1109/tgrs.2007.901027

Saatchi, S., 2019. SAR Methods for Mapping and Monitoring Forest Biomass, The Synthetic Aperture Radar (SAR) Handbook: Comprehensive Methodologies for Forest Monitoring and Biomass Estimation. NASA. https://doi.org/10.25966/hbm1-ej07

Simard, M., 2019. Radar Remote Sensing of Mangrove Forests, The Synthetic Aperture Radar (SAR) Handbook: Comprehensive Methodologies for Forest Monitoring and Biomass Estimation. NASA. https://doi.org/10.25966/33zm-x271

Weiß, T., 2019. SAR-Pre-processing Documentation.

Yommy, A.S., Liu, R., and Wu, A.S., 2015. SAR Image Despeckling Using Refined Lee Filter. 2015 7th Int. Conf. Intell. Human-Machine Syst. Cybern. https://doi.org/10.1109/ihmsc.2015.236